# Characterization of a 100 A-class LaB 6 hollow cathode for high-power Hall thrusters

Stéphane Mazouffre, Romain Joussot, Benjamin Vincent, Sedina Tsikata, S. Oriol, F. Masson

# Characterization of a 100 A-class $LaB_6$ hollow cathode for high-power Hall thrusters

**IEPC-2019-776**

*Presented at the 36th International Electric Propulsion Conference*
*University of Vienna, Austria*
*September 15-20, 2019*

S. Mazouffre* R. Joussot† B. Vincent‡ S. Tsikata§
*CNRS, ICARE laboratory, 1c Avenue de la Recherche Scientifique, 45071 Orléans, France*

*and*

S. Oriol¶ F. Masson‖
*CNES, Direction des Lanceurs, 52 rue Jacques Hillairet, 75612 Paris, France*

**This works deals with a laboratory model 100 A-class hollow cathode with a sintered lanthanum hexaboride ($LaB_6$) emitter for high-power Hall thrusters. The cathode has been fired up to 70 A with xenon as working gas. The cathode architecture, test set-up, ignition procedure and power consumption are described first. The second part of this contribution comments on the emitter temperature, the current-voltage characteristics and the discharge modes obtained for discharge currents in the 30–70 A range and mass flow rates in the 15–30 sccm range. Finally we present electron temperatures and densities measured in the cathode plasma plume by means of incoherent Thomson scattering.**

## Nomenclature

| | |
|---|---|
| $\alpha$, $A_0$ | Scattering parameter [-], Dushman constant [$A/cm^2/K^2$] |
| $d$ | Diameter [m] |
| $e$ | Elementary charge [C] |
| $I_d, I_h$ | Discharge, heater current [A] |
| $j$ | Current density [$A/m^2$] |
| $k$, $k_B$ | Wave vector [$m^{-1}$], Boltzmann constant [J/K] |
| $\lambda$, $\lambda_D$ | Wavelength [m], Debye length [m] |
| $n_e$ | Electron density [$m^{-3}$] |
| $\phi$ | Work function [eV] |
| $T$ | Temperature [K] |
| $\hat{T}_e$ | Electron temperature [eV] |
| $V_d$ | Cathode-to-Anode voltage [V] |
| $x$ | Position, distance [m] |

*Research Director, Head of the Electric Propulsion team, ICARE–CNRS, stephane.mazouffre@cnrs-orleans.fr
†Associate professor, University of Orléans
‡PhD student, Electric Propulsion team - ICARE–CNRS
§Research Scientist, Electric Propulsion team - ICARE–CNRS
¶PhD, Electric propulsion engineer, CNES
‖PhD, Electric propulsion engineer, CNES,

## I. Introduction

Hall thrusters are capable of providing large thrust with specific impulse levels far-above chemical propulsion ones during long time periods that can exceed 10000 hours.[1] High-power Hall thrusters operating in the 10 to 100 kW range are thus foreseen for applications such as orbit raising of heavy platforms as well as cargo and space tug missions in Earth and Moon orbits. The cathodes required for maintaining the plasma discharge and for ion beam neutralization of such large thrusters have to deliver a current in the 20 A to 300 A range depending on the specific impulse level while consuming several hundreds of Watts of power for heating.

Thermoionic hollow cathodes are a critical component for electrostatic propulsion devices as the electron current they emit is required for neutralization of the ion beam generated by the thruster.[1] Moreover, in the case of gridded ion engines and Hall thrusters cathode electrons also play a key role in ion production and plasma discharge sustainment.[2,3] The hollow cathode technology has greatly evolved and improved over the past decades thanks to advances in material science, manufacture processes and numerical simulations, see [2] and references herein. Available cathodes are stable and efficient, have a long lifespan and are able to operate in a wide range of discharge powers from a few Watts to several tens of kiloWatts.

Although studies and development of very high current hollow cathodes have started more than a decade ago, there is presently a large amount of works devoted to design optimization, efficiency and reliability improvement and lifetime extension in close relation with on-going projects on high power electric propulsion for deep space missions.[4–9] In this contribution, we present a prototype of a high-current hollow cathode with a lanthanum hexaboride ($LaB_6$) insert able to deliver up to 100 A of electron current. Thus far the cathode has been fired up to 70 A with xenon as working gas. After the description of the cathode architecture, we show and discuss results obtained during test campaigns with a dedicated set-up in terms of power consumption, emitter temperature, current-voltage characteristics, discharge modes and electron properties.

## II. Cathode architecture

A CAD as well as a cross-sectional view of the 100 A-class laboratory model $LaB_6$ cathode is shown in Fig. 1. The architecture is conventional and shares many common points with existing high-current devices.[5–9] As can be seen in Fig. 1, the cathode consists of two main parts: the base plate and the body that serves as keeper. The total length of the cathode, from the exit orifice to the base rear, is 154 mm. The base that includes electrical connections, gas feeding line and thermal and electrical insulator block is 75 mm in diameter and 40 mm in length. The external body, i.e. the keeper, has an outer diameter of 40 mm and a 114 mm length to accommodate the insert, the heater and heat shields. It is made of graphite. The cathode version used in this study has a 8 mm in diameter cathode orifice from which the plasma expands in the vacuum. The relatively large orifice diameter allows the electric field to penetrate inside the cathode and extract electrons. Electron emission is produced by a 25 mm in length and 12 mm in inner diameter sintered polycrystalline $LaB_6$ cylindrical insert, which provide an available emission area of 28.3 $cm^2$. The work function magnitude has been measured in the 100 °C to 1000 °C temperature range. It reaches 2.7 eV, a value very similar to the ones commonly found in the literature for $LaB_6$, see e.g. reference [8] and references therein. The $LaB_6$ emitter is inserted into a thin graphite tube with a 5 mm in diameter aperture to maintain a sufficiently high pressure inside the emitter which facilitates ignition and reduces gas flow rate. Note that graphite has a thermal expansion coefficient similar to the $LaB_6$ one, a very high melting point ($\sim$3600 °C), a good electrical conductivity and it does not suffer from boron diffusion. The insert is held in place by a graphite push-piece tube and a tungsten spring placed inside the graphite tube that contains the insert as shown in Fig. 1. The push-piece is sufficiently long and thin to minimize heat conduction from the insert to the base plate. Heating of the $LaB_6$ emitter is achieved by using a 0.6 mm in diameter tungsten wire axially wrapped around the graphite tube in the emitter region. The heater is electrically insulated with thin $Al_2O_3$ ceramic that has a maximum operation temperature about 1700 °C. Moreover this

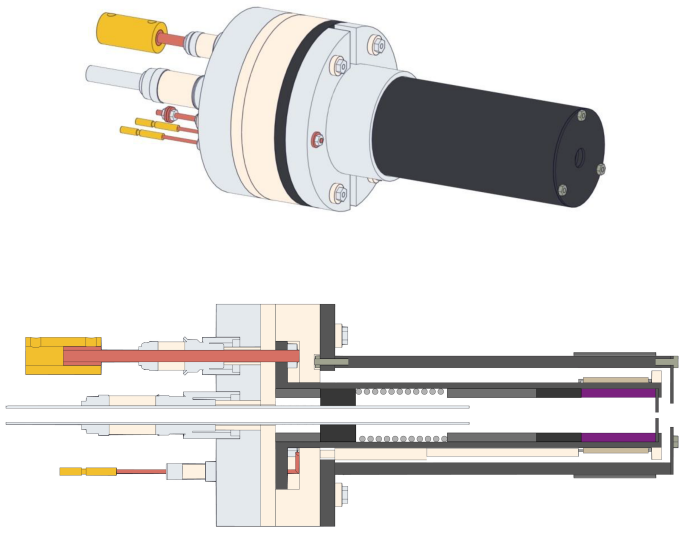

**Figure 1. CAD of the 100 A cathode developed at ICARE (top) and cross-sectional view showing main elements (bottom).**

ceramic is relatively stable and does not strongly react with the heater and heat shield material, which is necessary to reduce failure probability and reach a long operational life. A tantalum sleeve that surrounds the heater acts as a thermal shield. The thermal design of the cathode is critical to minimize heat losses and, consequently, the total amount of power required to start and operate the cathode. Therefore proper heat shielding of the cathode heater must warrant low radiative losses. In like manner, material and geometry of the various cathode components must warrant low heat conduction losses. An external igniter electrode has been added to the cathode to ease ignition. The igniter design is based on the one of the 5 A-class cathode studied in our laboratory.[10,11] The igniter is a 2 mm in diameter tungsten rod placed 2 mm downstream the cathode keeper orifice, as shown in Fig. 2. The igniter is slightly off-axis to minimize interaction with the expanding cathode plasma. At ignition the voltage is applied to the igniter during about 1 s to trigger electron extraction and switched to the anode afterwards.

## III. Experimental arrangement

The cathode has been operated with xenon in the NExET (New Experiments on Electric Thrusters) vacuum chamber in the so-called diode configuration[10] at discharge currents up to 70 A,

**Figure 2. External tungsten igniter.**

this limit being set by the 3 kW power supply. NExET is a stainless-steel vacuum chamber 1.8 m

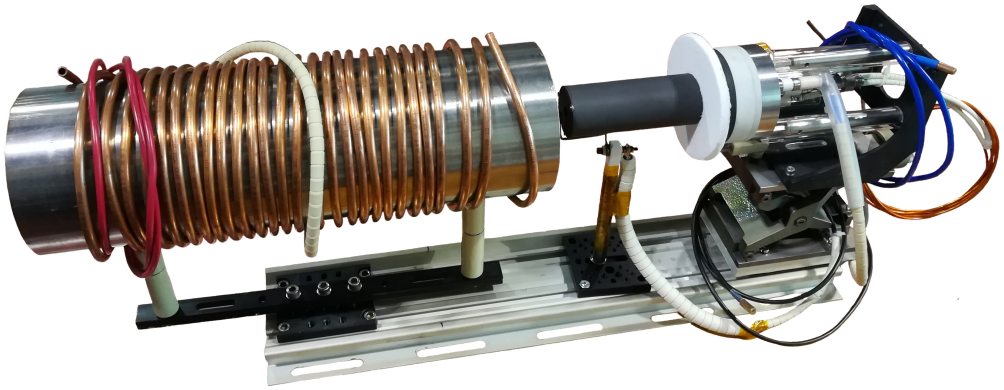

**Figure 3. Cathode test bench showing the water-cooled cylindrical anode located 2 cm downstream the cathode orifice.**

long and 0.8 m in diameter. It is equipped with a multistage pumping system that is composed of a large dry pump (400 $m^3$/h), a 350 l/s turbomolecular pump to evacuate light gases and a cryogenic pump with a typical surface temperature of $\sim 35$ K, which corresponds to about 8000 l/s, to remove gases such as xenon and krypton. A background pressure of about $5 \times 10^{-5}$ mbar-Xe is achieved with a xenon mass flow rate of 1.0 mg/s. The chamber is equipped with different observation windows, diagnostic ports as well as electrical and gas feed-throughs. The interior of the test bench is easy to access using a large front door.

The anode consists of a water-cooled stainless-steel cylinder 15 cm in diameter and 20 cm long that can handle the high-power discharge. The anode is placed 2 cm ahead of the cathode keeper orifice.[11] This configuration produces discharge voltages in the 15 to 25 V range and power up to 1100 W, depending on the current and gas flow rate. The cathode installed in the test setup along with the anode is shown in Fig. 3. Both the cathode and the anode are mounted on rails, as can be seen in the figure, which allows modification of the cathode-to-anode gap. The discharge current and cathode-to-anode voltage were applied with an Elektro-Automatik EA-PSI 9200-70 power supply able to deliver up to 170 A with a maximum output power of 5 kW. The power supply was mostly used in current-limited mode, which allows the voltage to adapt to the discharge need for stable operation. Heating of the $LaB_6$ emitter prior to ignition was controlled with high-current low-voltage power supply. Figure 4 is a photograph of the cathode operating with xenon at 30 A and 70 A. The discharge is in spot mode with low oscillation level at high currents.[10]

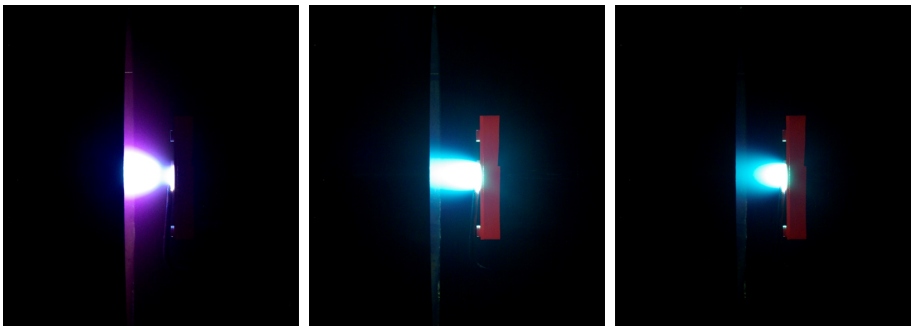

**Figure 4. Photograph of the cathode operating with xenon. From left to right: 30 A and 15 sccm (plume), 70 A and 15 sccm (spot), 70 A and 20 sccm (spot).**

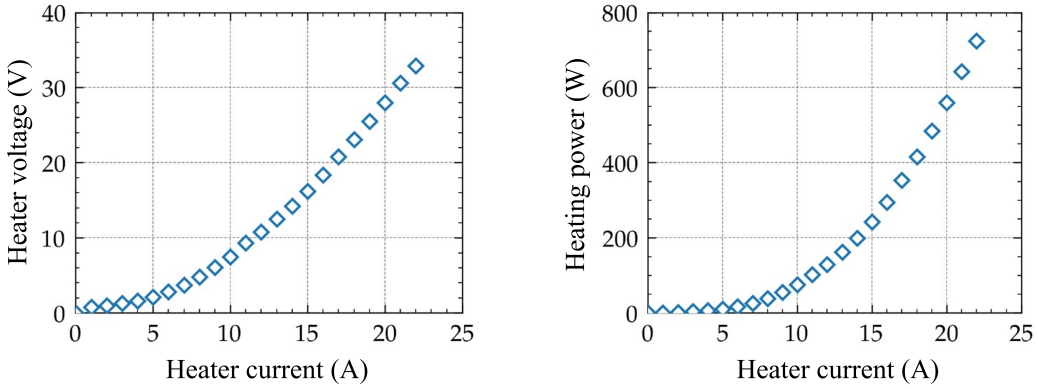


**Figure 5. Heater voltage (left) and power (right) against current.**

# IV. Experimental results

## A. Heating and ignition

### *1. Heater power*

Before starting experiments, the vacuum chamber is typically pumped down to $10^{-6}$ mbar. The heater current is slowly ramped up to about 25 A (1 A step every minute) before starting the plasma discharge. Figure 5 shows the cathode heater voltage and power as a function of the heater current. Ignition typically occurs around 23 A of current that means a heating power around 700 W. With the present design, ignition requires about 70 % of the discharge power. Improving thermal insulation to minimize heat losses and optimizing the $LaB_6$ insert geometry could certainly reduce the needed heating power below 500 W as achieved with other high-current cathodes.[6]

### *2. Emitter temperature*

The $LaB_6$ emitter temperature has been measured by means of electrically insulated type-C thermocouples during the heating phase prior to ignition and during operation for various xenon flow rates and discharge currents. The thermocouples are embedded into the cathode structure and in contact with the external surface of the emitter. The temperature has been recorded at 3 different axial locations to examine energy deposition inside the emitter, as shown in Fig. 6. The

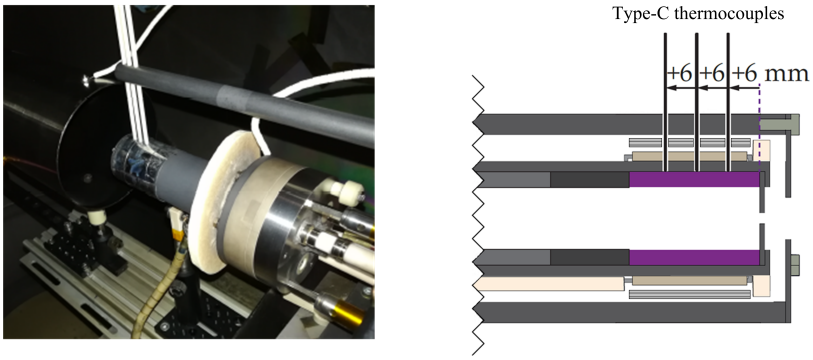


**Figure 6. Photograph of the 3 type-C thermocouples used to measure the emitter temperature (left). Layout of the thermocouple assembly (right).**

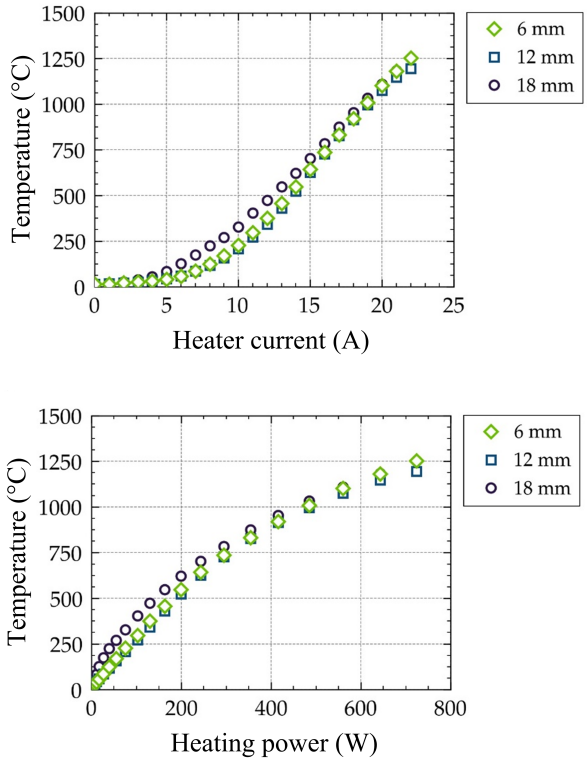


**Figure 7. Evolution of the $LaB_6$ emitter temperature as a function of the heater current (top) and heater power (bottom). Thermocouples are located at 6, 12 and 18 mm where 0 refers to the emitter exit orifice.**

thermocouples at located at $x = 6$, 12 and 18 mm of the $LaB_6$ insert edge as illustrated in Fig. 6. The thermocouple positions correspond to $x/d_{in} = 0.5$, 1 and 1.5, respectively, where $d_{in}$ is the emitter inner diameter. The cathode base plate temperature has been monitored using type-K thermocouples to assess thermal losses due to heat conduction. The anode temperature was also recorded with a type-K thermocouple placed 2 cm downstream the anode inlet.

Figure 7 illustrates the evolution of the $LaB_6$ emitter temperature at 6, 12 and 18 mm as a function of the heater current and heater power. Above 20 A, that corresponds to about 600 W of heating power, the emitter temperature is relatively homogeneous. It reaches about 1200 °C at 23 A. Thermionic emission by polycrystalline sintered $LaB_6$ can be described by the Richardson–Dushman equation:[12,13]

$$j = A_0 T^2 \exp\left(-\frac{e\phi}{k_B T}\right), \tag{1}$$

where $j$ is the emission current density, $A_0$ is the Dushman constant of which the theoretical value is 120.4 A/cm$^2$/K$^2$,[12,14] $T$ is the surface temperature, $e$ is the elementary charge, $k_B$ is the Boltzman's constant and $\phi$ is the work function. With an active emission area of 28.3 cm$^2$ and a work function of 2.7 eV the cathode should emit 4 A, respectively 235 A, at a temperature of 1200 °C, respectively 1500 °C, assuming the surface temperature is perfectly homogeneous over the whole insert length. Using a lower Dushman coefficient, typically around 30 A/cm$^2$/K$^2$ for sintered $LaB_6$,[14] leads to a smaller emitted current.

The change of the base plate and anode temperature as a function of the heater current and heater power is shown in Fig. 8. Whereas the anode temperature always remains below 300 °C, the base plate temperature exceeds 500 °C at 20 A due to heat transfer by conduction from the emitter region. Such a high temperature indicates heat is poorly confined in the final section of

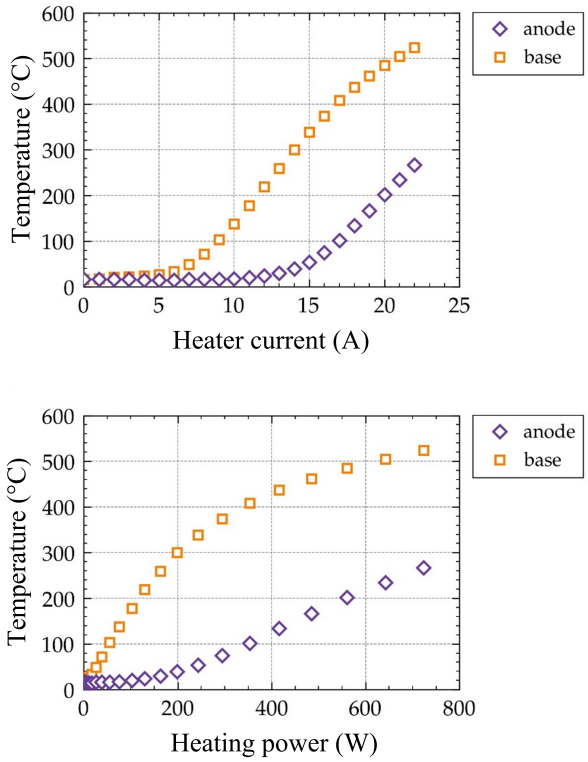


**Figure 8. Evolution of the base plate and anode temperature as a function of the heater current (top) and heater power (bottom).**

the cathode. The relatively large base plate temperature is a direct consequence of the high power needed to reach an elevated emitter temperature. On the contrary the anode can easily evacuate heat due to its large surface area, hence a low temperature. Notice the anode was not water-cooled during these experiments.

### *3. Ignition*

When the $LaB_6$ emitter is sufficiently hot ($I_h \approx 23\,A$) the plasma discharge is started in the same manner as with low-power cathodes by injecting the xenon gas through the cathode, applying a relatively large voltage to the igniter electrode and turning on the power supply. Quiet and smooth ignition along with stable discharge with low oscillation level was reached with the following parameters: 30 mg/s xenon mass flow rate, anode voltage limited to 200 V, discharge current fixed to 50 A and external igniter electrode voltage and current limited to 400 V and 2 A respectively. The igniter discharge was power with a Delta Elektronika SM 400-AR-8 (400 V, 4 A) power supplies. The cathode discharge and igniter power supplies are connected in paralell. All power supplies share a common ground. Note that no electrical current flows through the keeper electrode (body) during ignition. After ignition of the cathode discharge, the igniter voltage is switched off. After about 5 mn, the heater current is quickly decreased to zero. In this work the cathode was always operated with no additional heating, i.e. it works in selfheating regime. As soon as the heater is turned off the flow rate and current are set to the target value.

## B. Emitter temperature during operation

The type-C thermocouples have been used to measure the $LaB_6$ insert temperature at different positions during cathodes functioning. Figure 9 shows the emitter temperature as a function of

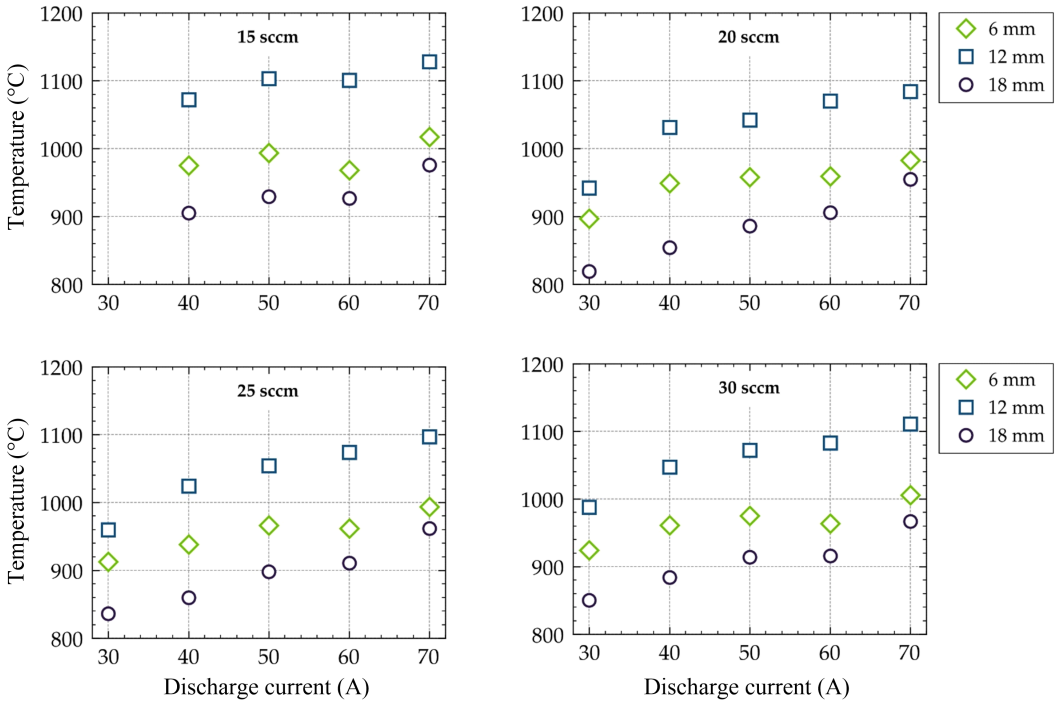


**Figure 9. Emitter temperature against discharge current for 4 xenon mass flow rates.**

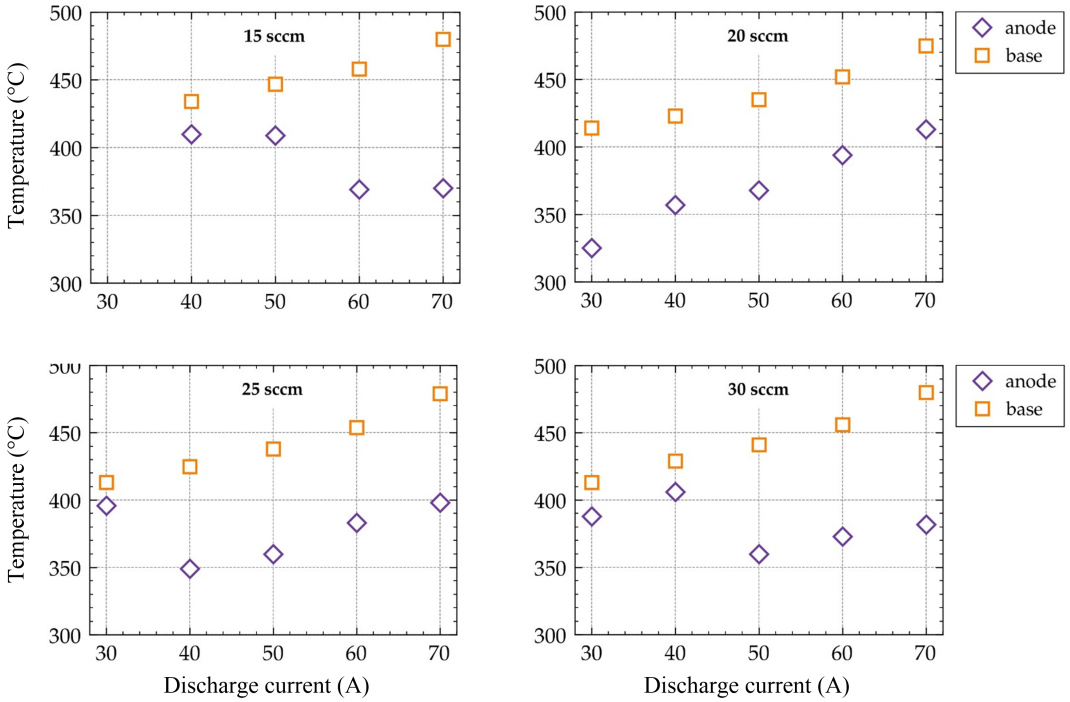


**Figure 10. Base plate and anode temperature against discharge current for 4 xenon mass flow rates.**

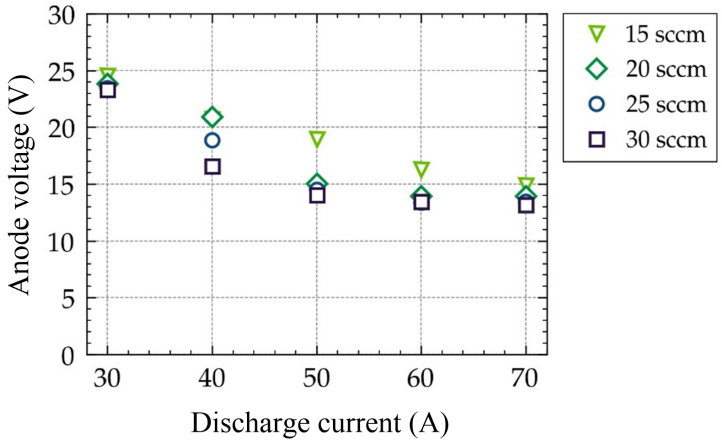


**Figure 11. Current–voltage characteristics for various flow rates.**

the discharge current for 4 values of the xenon mass flow rate. Measured temperatures are surprisingly low. According to equation 1, with such a temperature the emitter is unable to produce a current above 1 A, which obviously contradicts observations.

There are several possible explanations for the measured low emitter temperature. Firstly, a large heat resistance at the contact point between the thermocouples and the external emitter surface or no direct physical contact at all, due to e.g. thermal expansion of elements, leads to underestimate the temperature. This technical defect must, however, be comparable for the three thermocouples. Secondly, a large temperature gradient across the $LaB_6$ cylinder layer (several 100s K) would induce a greater inner surface temperature. Finally, electron extraction from the $LaB_6$ surface would be facilitated by an additional Schottky effect, hence a low temperature. Under our conditions, production of several tens of Ampers nevertheless requires an electric field strength in excess of $10^8$ V/m at 1000 °C, which is unlikely.

The trend that is observed in Fig. 9 is the expected one. The emitter temperature increases when the discharge current is ramped up. Moreover the temperature is not much affected by the gas flow. Measurements show a relatively strong temperature gradient in the axial direction, with a maximum temperature around $x = 12$ mm, whatever the operating conditions. This result indicates the plasma discharge is concentrated in the middle of the insert, as observed in numerical simulations.[15]

The base plate and anode temperature are illustrated in Fig. 10 for several conditions. The base plate temperature is around 450 °C, which corresponds to an emitter external surface temperature of about 1000 °C according to the plot in Fig. 7. The base temperature increases with the discharge current and it is not much affected by the gas flow rate. Measurements during the heating phase and during heaterless cathode operation are fully consistent. The anode temperature varies between 350 and 400 °C. The abrupt changes in temperature at 15 mg/s and 30 mg/s might be connected with mode transitions, see next section.

### C. Current–voltage characteristics

The discharge current and anode voltage time series have been recorded in steady state by way of a calibrated high-frequency voltage probe (Tektronix P6139A, 500 MHz) and a calibrated Rogowski coil current probe (Stangenes Model 0.5-0.1W,35 MHz, 500 A peak) respectively for xenon flow rates in the 15 sccm to 30 sccm range and current in the 30 A to 70 A range. Notice the mean value of $I_d$ is read on the power supply display. Figure 11 shows voltage–curent characteristics of the 100 A cathode for four different gas flow rates. The evolution of the anode voltage as a function of the flow rate is displayed in Fig. 12 for a discharge current varying from 10 A up to 70 A.

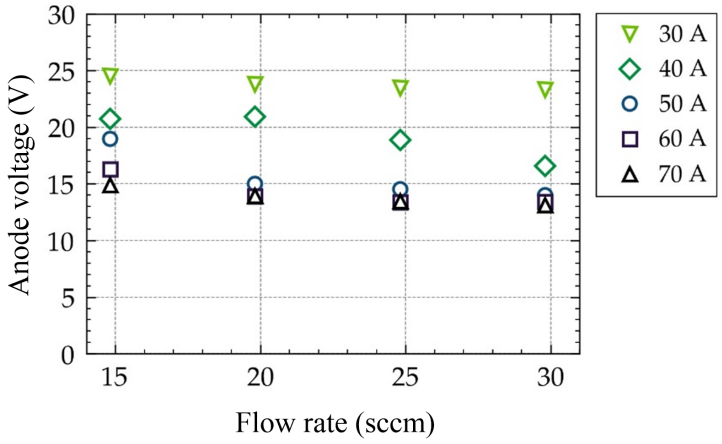


**Figure 12. Anode voltage against flow rate from 30 A to 70 A.**

The two figures correspond to two different graphic representations of the same date set. They indicate that the discharge power reaches 750 W at 30 A and ∼1 kW at 70 A. As can be seen in Fig.11 and 12, the anode voltage decreases when the current increases and it stays in the [10–25] V range, in agreement with outcomes of preceding studies.[6,8,16,17] The self-heating regime of hollow cathodes depends on the discharge current magnitude.[3] According to the Richardson-Dushman relation electron current generation is linked to the emitter surface temperature. As low discharge currents provide insufficient heating, the discharge voltage increases to create high kinetic energy ions which maintain the appropriate emitter temperature.

The cathode operation mode cannot be determined in a reliable manner from visual inspection of the plume, see Fig. 4, or from the current and voltage mean value even though the voltage is often large in plume mode. The proper approach for the determination of the discharge mode rests upon calculation of the current and voltage time series standard deviation, which characterizes the fluctuation level, see[10,11] and references herein. Large amplitude current fluctuations are indeed associated with the plume mode. More specifically, when the current fluctuation to mean value ratio is below 0.09 a cathode operates in spot mode according to many works.

Figure 13 shows the voltage and the current standard deviation as a function of the discharge current for a xenon flow rate varying from 15 sccm to 30 sccm. The current standard deviation is plotted in Fig. 14 against the gas lfow rate from current in the [30–70] A range. The two figures

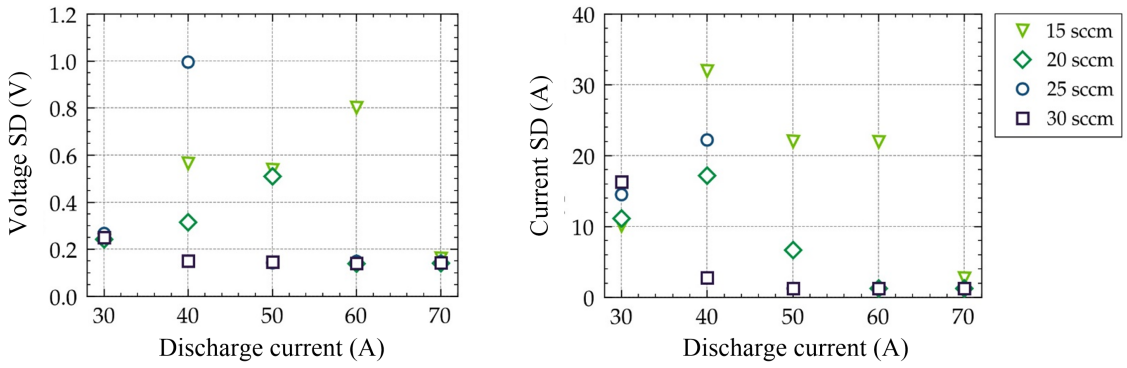


**Figure 13. Voltage (left) and current (right) standard deviation as a function of $I_d$ for various xenon gas flow rate.**

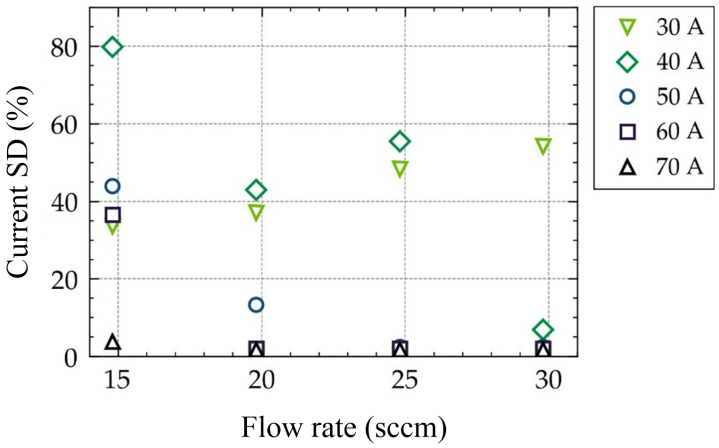


**Figure 14. Discharge current standard deviation in percent against xenon gas flow rate from 30 A to 70 A.**

indicate that the discharge is in spot mode when $I_d$ is larger than 40 A at 25 sccm and when $I_d$ is larger than 30 A at 30 sccm. At 15 sccm, respectively 20 sccm, the discharge operates in spot mode when $I_d$ is larger than 50 A, respectively 70 A. Those results agree with results obtained with other high current cathodes.[2,6,9] Figure 14 shows that the cathode discharge is always in spot mode at $I_d = 70$ A whatever the flow rate. Therefore operation in spot mode might be possible with low flow rates above 70 A. In brief, the cathode operates in plume mode at low mass flow rates and low currents and in spot mode at large flow rates and large currents.

### D. Electron properties in the plume

Electron temperature and density have been measured downstream the cathode exit plane by means of incoherent Thomson scattering (ITS), a non-invasive, direct and spatially-resolved laser-aided diagnostic technique.[18,19] Thomson scattering is the scattering of incident electromagnetic radiation on free electrons, which allows the direct observation of the Electron Energy Distribution Function (EEDF) in the direction of the wave vector $\mathbf{k}$ defined according to the Bragg relation: $\mathbf{k} = \mathbf{k_s} - \mathbf{k_i}$, where $\mathbf{k_s}$ and $\mathbf{k_i}$ are the scattering and incident wave vectors, respectively. Two scattering regimes can be distinguished according to the scattering parameter $\alpha = 1/k\lambda_D$, where $\lambda_D$ is the Debye length. When $\alpha < 1$ the scattering regime is incoherent: the scattering length scales are shorter than the electron screening length. In that case individual electron fluctuations can be observed, allowing electron density and temperature to be determined.

Details about the compact high-sensitivity ITS bench used in this study can be found in reference.[20] Only a short description is given here. Coherent light is produced by a 10 Hz Nd:YAG laser (Quantel Q-Smart 850) able to deliver up to 430 mJ per pulse at 532 nm. Several high-reflectivity optics are used to transmit light to the observation volume. Brewster windows mounted at the end of long tubes minimize the stray light level. In the center of the plasma volume, the beam waist is about 0.3 mm. After traversing the plasma, the beam is sent to a beam dump with a large acceptance aperture. Scattered radiation is collected perpendicular to the incident beam direction. A fiber bundle consisting of 45 multi-mode fused silica fibers transfers light from the scattering volume to a spectrometer. A spectrally-narrow, high transmission Volume Bragg Grating (VBG) notch filter is used to significantly attenuate stray light and Rayleigh-scattered light at 532 nm instead of the usual double- or triple-grating spectrometers with masks. A Princeton Instruments Acton SP-2750 spectrometer fitted with silver-coated mirrors disperses the collected light. The detector is a Princeton Instruments ICCD PI-MAX4: 1024f camera. The combined spectrometer and camera features provide a full wavelength coverage at 532 nm of 5.1 nm

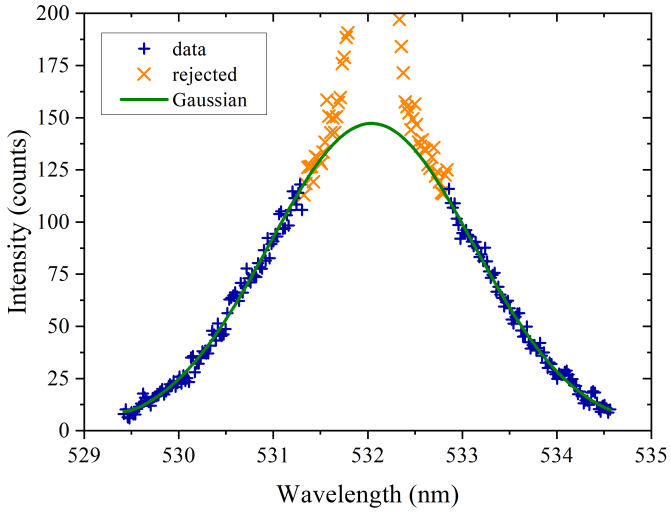


**Figure 15. Thomson scattering spectrum measured at $x = 10$ mm with the cathode operating at 50 A and 30 sccm (350 mJ, 6000 laser pulses).**

and 28.6 nm, respectively, for the 2400 lines mm$^{-1}$ and 600 lines mm$^{-1}$ grating. The ITS diagnostic is calibrated using nitrogen Raman spectra measured at relatively low pressures (∼10 mbar. In this work the optical configuration in terms of $k$ vectors allows the observation of the EEDF in the radial direction.

Figure 15 show an incoherent Thomson scattering spectrum obtained in the plume of the 100 A-class cathode firing at 50 A with 30 sccm xenon flow rate. Acquisition has been performed with a laser pulse energy of 350 mJ and using averaging over 6000 laser shots. As can be seen, stray and Rayleigh light at 532 nm is strongly attenuated. Experimental data points are fitted to a Gaussian function to extract electron properties. The ITS spectrum in Fig. 15 gives values of electron temperature and density of, respectively, 2.1 eV and $7.6 \times 10^{17}$ m$^{-3}$.

ITS spectra have been recorded along the cathode centerline for several discharge conditions: 30 A (15 sccm), 40 A (30 sccm) and 70 A (30 sccm). Cathode parameters, background pressure in the NExET vacuum chamber and discharge mode are summarized in table 1. Figure 16 shows the on-axis development of the electron density $n_e$ and the electron temperature $T_e$ for 30 A, 40 A and 70 A. The position $x = 0$ refers to the cathode keeper orifice. The cathode-to-anode distance is 2 cm. The electron density decreases along the cathode plume centerline in all cases. Three mechanisms can explain the measurement outcomes, namely: acceleration of the electron fluid, increase in the plume divergence angle with the distance to the orifice or recombination losses. The last mechanism is unlikely under our conditions (low pressure). The electron density drastically increases with the cathode current. At $x = 5$ mm $n_e$ varies from $\sim 6 \times 10^{17}$ m$^{-3}$ at 30 A to $\sim 5 \times 10^{18}$ m$^{-3}$. Notice that at 70 A, $n_e$ is far above $10^{18}$ m$^{-3}$ behind the cathode outlet.

**Table 1. Cathode parameters, pressure and mode.**

| Flow rate sccm | $I_d$ A | $V_d$ V | Power W | Pressure mbar | Mode |
|---|---|---|---|---|---|
| 15 | 30 | 22,2 | 666 | $1{,}2\times10^{-4}$ | plume |
| 30 | 40 | 14,6 | 584 | $1{,}2\times10^{-4}$ | spot |
| 30 | 70 | 15,3 | 1071 | $7{,}8\times10^{-5}$ | spot |

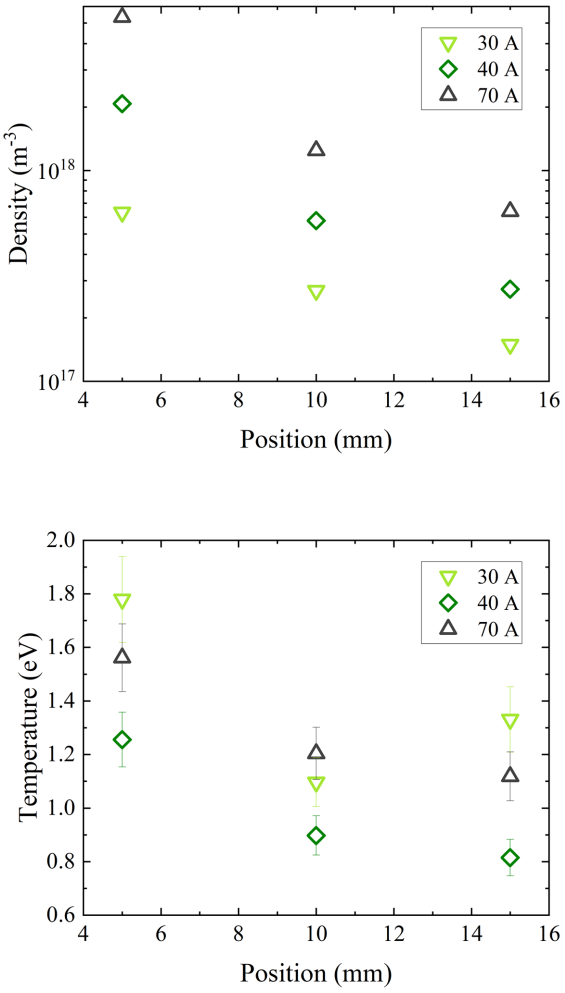


**Figure 16. Electron density (top) and temperature (bottom) along the cathode centerline at 30 A, 40 A and 70 A.** $x = 0$ **mm refers to the cathode orifice. Cathode characteristics are given in Tab. 1.**

As can be seen in Fig. 16, the electron temperature is relatively low, even at high cathode current. This result is in agreement with measurements performed with a cylindrical Langmuir probe in the plume of a high current cathode operating at 50 A.[21] Langmuir probe measurements in the plume of a flat disk $LaB_6$ emitter hollow cathode give an electron temperature around $\sim 1.3$ eV in spot mode at 4 A discharge current with 0.6 mg/s xenon mass flow rate.[11] ITS measurements carried out 1.3 mm downstream the orifice of the same cathode indicate a temperature of 2.2 eV and a density of $9 \times 10^{17}$ m$^{-3}$ at 16 A discharge current and 8 sccm (spot mode)[20]

The electron cooling along the cathode plume centerline that can be observed behind the cathode keeper orifice for all currents in Fig. 16 certainly originates in energy transfer through collision events and plasma flow expansion.[22]

As can be seen in Fig. 16 the highest electron temperature is reached at $x = 5$ mm at 30 A cathode discharge current and not 70 A as one could expect. This fact is certainly linked to the xenon gas flow rate, which is only 15 sccm at 30 A as indicated in Tab. 1. As the gas density is low, energy transfers are weaker, hence a large temperature. Moreover the cathode operates in plume mode at 30 A and 15 sccm, which leads to a large voltage and strong current oscillations,

as shown previously, see Fig. 11–14, which favors electron heating.

## V. Conclusion

A laboratory model 100 A-class hollow cathode with a sintered lanthanum hexaboride ($LaB_6$) emitter has been tested up to 70 A with xenon. The cathode operates in spot mode at high currents with very low discharge current oscillations whereas it operates in plume mode with large oscillation amplitude at low currents.

Electron temperatures and densities have been measured downstream the cathode keeper orifice by means of incoherent Thomson scattering instead of Langmuir probes. Densities are large ($> 10^{18}\,m^{-3}$) and strongly depends upon the current level. On the contrary temperatures are relatively low around 1.5 eV despite the large current level.

## Acknowledgments

This work was financially supported by the CNES Direction des Lanceurs Research and Technology program under grant 161265/00.

## References

[1]S. Mazouffre, "Electric propulsion for satellites and spacecraft: established technologies and novel approaches", *Plasma Sources Sci. Technol.* 25, 2016 033002.

[2]D. R. Lev, I. G. Mikellides, D. Pedrini, D. M. Goebel, B. A. Jorns, M. S. McDonald, "Recent progress in research and development of hollow cathodes for electric propulsion", *Rev. Mod. Plasma Phys.*, 2019, 3:6.

[3]D. M. Goebel, I. Katz, *Fundamentals of Electric Propulsion*, Wiley, Hoboken (NJ), 2008, pp. 243–323.

[4]L. Garrigues et al, "Design of a 100 A-class $Lab_6$ cathode for high-power electric propulsion", *Proceedings of the Space Propulsion conference*, Seville, Spain, 2018, SP2018-473.

[5]D. Pedrini, R. Albertoni, F. Paganucci, M. Andrenucci, "Development of a $LaB_6$ cathode for high-power Hall thrusters", *Proceedings of the 34th International Electric Propulsion Conference*, Hyogo-Kobe, Japan, 2015, IEPC paper 2015-47.

[6]E. Chu and D. M. Goebel, "High-current lanthanum hexaboride hollow cathode for 10-to-50-kW Hall thrusters", *IEEE Trans. Plasma Sci.* 40, 2012, pp. 2133–2144..

[7]D. M. Goebel, R. M. Watkins, K. K. Jameson, "$LaB_6$ hollow cathodes for ion and Hall thrusters", *J. Propul. Power* 23, 2007, pp. 552–558

[8]D. M. Goebel and E. Chu, "High-current lanthanum hexaboride hollow cathode for high-power Hall thrusters", *J. Propul. Power* 30, 2014, pp. 35–40.

[9]D. M. Goebel, G. Becatti, S. Reilly, K. Tilley, S. J. Hall, "High current lanthanum hexaboride hollow cathode for 20-200 kW Hall thrusters", *Proceedings of the 35th International Electric Propulsion Conference*, Atlanta, Georgia, 2017, IEPC paper 2017-303.

[10]R. Joussot, L. Grimaud, S. Mazouffre, "Examination of a 5 A-class cathode with a $LaB_6$ flat disk emitter in the 2 A–20 A current range" *Vacuum* 146, 2017, pp.52–62.

[11]G.-C. Potrivitu, R. Joussot, S. Mazouffre, "Anode position influence on discharge modes of a $LaB_6$ cathode in diode configuration", *Vacuum* 151, 2018, pp. 122–132.

[12]J. M. Rax, *Physique de la conversion d'énergie* EDP Sciences, CNRS édition, 2015, pp. 191–234.

[13]M.E. Kiziroglou, X. Li, A. A. Zhukov, P. A. J. de Groot, C.H. de Groot, "Thermionic field emission at electrodeposited Ni–Si Schottky barriers", *Solid-State Electronics* 52, 2008 pp. 1032-–1038.

[14]J. Pelletier, C. Pomot, "Work function of sintered lanthanum hexaboride", *Appl. Phys. Lett.* 34, 1979, pp. 249–251.

[15]I. G. Mikellides, D. M. Goebel, B. A. Jorns, J. E. Polk, P. Guerrero, "Numerical Simulations of the Partially-ionized Gas in a 100-A $LaB_6$ Hollow Cathode", *Proceedings of the 33rd International Electric Propulsion Conference*", Washington, D.C., IEPC Paper 2013-142.

[16]D. Pedrini, R. Albertoni, F. Paganucci, M. Andrenucci, "Experimental characterization of a lanthanum hexaboride hollow cathode for five-kilowatt-class Hall thrusters", . *J. Propul. Power* 32, 2016 pp. 1557—-561.

[17]K. Kubota, Y. Oshio, H. Watanabe, S. Cho, Y. Ohkawa, I. Funaki, "Numerical and experimental study on discharge characteristics of high-current hollow cathode", *Proceedings of the 52nd Joint Propulsion Conference*, Salt Lake City, UT, 2016, AIAA paper 2016-4628.

[18]J. Sheffield, D. Froula, S. H. Glenzer, N. C. Luhmann, Jr., *Plasma Scattering of Electromagnetic Radiation – Theory and Measurement Techniques*, Academic Press, Elsevier, 2011

[19]I. H. Hutchinson, *Principles of Plasma Diagnostics*, Cambridge University Press, 2001, pp. 273–321.

[20]B. Vincent, S Tsikata, S. Mazouffre, T. Minea, J. Fils, "A compact new incoherent Thomson scattering diagnostic for low-temperature plasma studies", *Plasma Sources Sci. Technol.* 27, 2018, 055002.

[21]R. E. Thomas, H. Kamhawi, G. J. Williams, Jr, "High current hollow cathode plasma plume measurements", *Proceedings of the 33rd International Electric Propulsion Conference*, Washington, DC, 2013, IEPC paper 2013-076.

[22]R. van de Sanden, *The expanding plasma jet : Experiments and model*, PhD thesis, Eindhoven University of Technology, The Netherlands, 1991.